EMT Implementation and Validation of MPC for VSC-HVDC Embedded in AC Meshed Grid

Emile Thau, Elkhatib Kamal, Bogdan Marinescu, Guillaume Denis

EMT Implementation and Validation of MPC for VSC-HVDC Embedded in AC Meshed Grid

Emile Thau
Ecole Centrale de Nantes - LS2N, France
emile.thau@ec-nantes.fr

Elkhatib Kamal
Ecole Centrale de Nantes - LS2N, France
elkhatib.ibrahim@ec-nantes.fr

Bogdan Marinescu
Ecole Centrale de Nantes - LS2N, France
bogdan.marinescu@ec-nantes.fr

Guillaume Denis
RTE - R&D, France
guillaume.denis@rte-france.com

***Abstract*—This paper proposes a Model Predictive Control (MPC) for a High Voltage Direct Current (HVDC) inserted in an AC network, in order to improve the dynamic behavior performance under input and state non symmetrical constraints. To fully capture all range of grid and converter dynamics, an Electromagnetic Transients (EMT) modeling is done. For this, the well known New-England test case is enriched by adding a HVDC link. For the latter, a MPC is synthesized based on Linear Matrix Inequalities (LMIs) conditions for stabilization, in the sense of the Lyapunov theory. Constraints for converters currents are also integrated into the design in order to obtain a control implementable in practice. The proposed strategy is then compared with classic vector control to show the effectiveness of the strategy. Simulations are performed in EMT MATLAB/Simulink/Simpower/Simscape software environment.**

***Index Terms*—Asymmetrical constraint, EMT, HVDC, MPC, VSC.**

I. Introduction

High Voltage Direct Current (HVDC) transmission systems are getting more widely used as modern and environmental acceptable technology to reinforce the transmission grid. Voltage Source Converter (VSC) based HVDC transmission (VSC-HVDC) has several technical advantages compared to the conventional, thyristor based, HVDC (i.e., it can supply inductive or capacitive reactive power to the grid, has high speed and high voltage switches [1]).

When inserted into a *meshed* AC grid, the HVDC converters and regulations may interact with other dynamic elements in the neighbour. To avoid oscillations and to improve transient stability of the neighbour zone, the control specification should be enlarged to AC grid transients [2]. To satisfy such enhanced specifications, some cautions may be taken into the HVDC control synthesis. It has been shown in [2] and related references that one should consider an *extended control model* which should capture not only the HVDC dynamics, but also some features of the grid. The simplest control model is the one used in [3] which incorporates equivalent grid impedances seen from the HVDC terminals. In that work, the simulation model was assimilated to the control model. The control model presented in this paper is extracted from a realistic model of a power system.

In addition, controller design for state and actuator constrained VSC-HVDC systems is a challenging issue. Several authors have presented mathematical models and control strategies for VSC-HVDC transmission that include small-signal stability [4], decoupling control in converter stations using feedback linearisation [5], Linear Matrix Inequalities (LMI) based robust control [6], [7], and adaptive control [8]. These papers have not considered the constraints on physical variables (e.g. converter currents). In many control systems, including VSC-HVDC links, input saturation is often the cause of performance degradation or even instability [9]. Hence, stabilization of such systems is typically achieved by considering the input saturation during the synthesis of the controller [10], [11].

A powerful method to directly handle constraints, on the input or on the state, is Model Predictive Control (MPC). Due to the significant increase of computational power of microprocessors, the interest on this topic has dramatically grown over the last decades, including in the field of power electronics [12], [13]. A preliminary synthesis for the HVDC control specifications mentioned above was presented in [3]. In this paper, this work is extended to fully take into account Electromagnetic Transients (EMT) dynamics and to apply to a realistic power system. For this, an EMT benchmark has been created by inserting a HVDC into the well-known New-England (NE) system. It is shown first how the appropriate control model is extracted from the whole power system model and, next, how this control model is used to synthesise the MPC control law. Hence, the main contribution of this paper is the validation of a MPC controller [3] on a realistic EMT meshed AC grid.

The paper is organized as follows: In Section II, an EMT New England modified benchmark with VSC-HVDC link is depicted. Section III presents the problem formulation. Then, Section IV proposes a control model and a control strategy based on MPC with state and control constraints. In Section V, this strategy is validated via simulation and compared with vector control. Finally, Section VI reports the conclusions.

II. Modelling of a VSC-HVDC link embedded in the New England grid

In order to analyse the performance of a VSC-HVDC controller, its insertion in a realistic network is important. Indeed, HVDC models connected to infinite nodes cannot take into account the synchronous machines dynamics or inter-area modes. This section will focus on the New England 10 machines network, which fits well these needs (see e.g. [14]), and the modelling of the VSC-HVDC that has been inserted in it. These models have been implemented on MATLAB/Simulink/Simscape in EMT.

A. The New England grid

The NE grid is a 39-bus grid that includes 10 synchronous machines. Its topology is shown in Fig. 1. It has been selected for its medium scale, that allows a good variety of network dynamics and a reasonable computation cost. Note that the NE grid does not originally include a HVDC link.

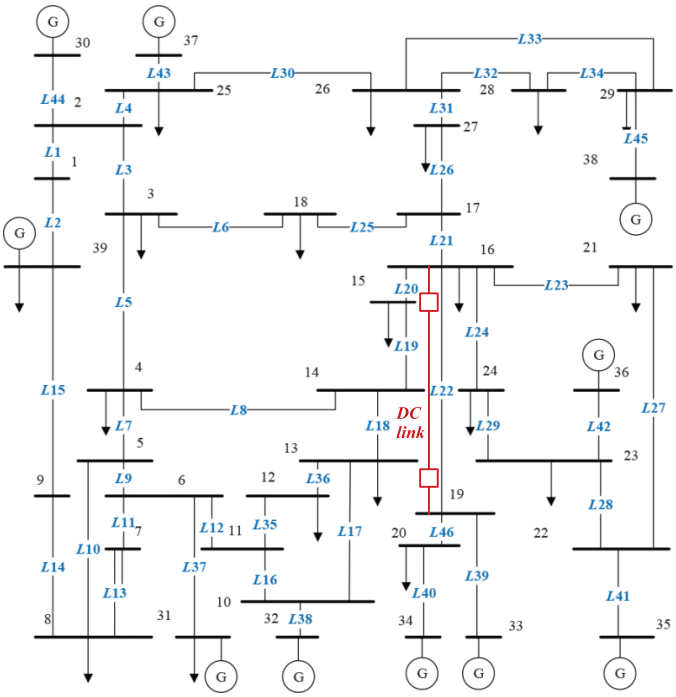

Fig. 1. New England 39-bus network [14]

B. VSC-HVDC modelling

A VSC-HVDC link is considered, with two conversion stations employing bidirection three-phased (voltage-source) AC-DC power converters, interlinked by a DC cable. Each converter is connected to the grid through an AC filter impedance and a transformer. DC filters are also modelled. The filters have been adapted to this test case with attention paid to the per unit consistency regarding the nominal values of the VSC-HVDC link. The first VSC station of the VSC-HVDC link is shown in Fig. 2. The second station has identical parameters. The local variables are measured by a Phase-Locked Loop (PLL) including a PI controller [15]. An average model represents the converters [16], implementing in dq coordinates the following equations:

$$\begin{aligned} v_{1d} &= \tfrac{1}{2}\beta_{1d}v_{DC1} \quad & v_{1q} &= \tfrac{1}{2}\beta_{1q}v_{DC1} \\ v_{2d} &= \tfrac{1}{2}\beta_{2d}v_{DC2} \quad & v_{2q} &= \tfrac{1}{2}\beta_{2q}v_{DC2} \end{aligned} \tag{1}$$

Where β are the control inputs of the VSC stations, v_{DC1} and v_{DC2} are the DC voltages at each side, v_1 and v_2 are the AC voltages of the converters. i_1 and i_2 are the AC converter currents. The HVDC link is inserted in the NE grid, in parallel of an AC line, is between buses 19 and 16 (see Fig.1).

III. Problem Formulation

The objective here is to design a controller for the HVDC system that meets the following criteria :

1) Enforce control constraints [16] :

$$-1 \leq \beta_{1d}, \beta_{1q}, \beta_{2d}, \beta_{2q} \leq 1 \tag{2}$$

and state constraints, defined by squared approximation:

$$\begin{aligned} -2000A \leq i_{1d}, i_{1q}, i_{2d}, i_{2q}, i_{DC} \leq 2000A \\ 260kV \leq v_{DC1}, v_{DC2} \leq 340kV \end{aligned} \tag{3}$$

Note that the control constraints are hard constraints, linked to a saturation, whereas the state constraints are soft constraints that as to be ensured by the controller.

2) Ensure the tracking of the DC voltage v_{DC1} of the first converter, the active power P_2 of the second converter, and the reactive powers Q_1 Q_2 of both, to their set points, with no overshoot and a response time of about $100ms$, which is usual for commercial DC links. Thus, the tracking error tends to zero as time goes to infinity.

IV. MPC with State and Control Constraints Strategy

In this section, a MPC controller synthesis based on LMI [17]–[21] is detailled, to fit the criteria listed in section III . This controller is detailled in [3], but a difference is noteworthy. The control model is here broaden to include AC filters and transformers, while keeping the same state size and variables. Hence, the modelling errors are reduced, and the computation complexity stays the same.

A. Control Model

1) General Scheme: A control model has to integrate some dynamics induced by the insertion of the HVDC link in an AC grid while having a small complexity. The proposed control model (Fig. 3), more straightforward than a dynamic grid reduction approach [22], has a detailed representation of the HVDC, and the AC grid is represented only by equivalent impedances. It includes AC filters and transformers. The parallel AC line is crucial to portray the meshed AC grid. The VSC-HVDC is here represented by an averaged model, neglecting its switching dynamics [16]. The transformers impedances of the real model can be easily merged with the AC filter impedances of the control model, (L_{S1}, r_{S1}) and (L_{S2}, r_{S2}). Part of the DC filter can be included in the DC line parameters (L_{DC}, r_{DC}), C_1 and C_2. Lg_1, Lg_2 and L_{AC} are equivalent

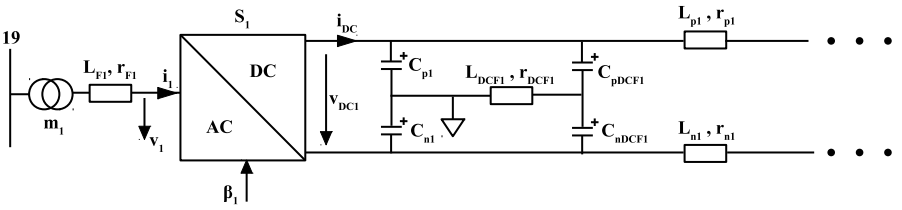

Fig. 2. Station 1 of HVDC with transformer, AC filter and DC filter

lines that represent the grid. Their computation is detailed below.

2) Identification of the equivalent AC inductances: To identify the equivalent lines Lg_1, Lg_2 and L_{AC}, the equivalent grid around buses 19 and 16 is considered. This system is depicted in Fig. 4. The inductances are assumed to be under a voltage of $V = 345kV$, modelled by infinite buses. The parameters of the control model are then identified in simulation in 2 steps:

1) Two simultaneous short-circuits are applied at buses 19 and 16 of *the real NE grid*, without HVDC. The steady-state short-circuit currents I_{cc1} and I_{cc2} are measured. (cf. Fig. 5). Since there is no current on the line 19-16, L_{g1} and L_{g2} are given by:
$$L_{g1} = \frac{V}{I_{cc1}\omega} \qquad L_{g2} = \frac{V}{I_{cc2\omega}} \tag{4}$$
with $\omega = 2\pi f$ and $f = 50Hz$
2) A short circuit is applied at bus 16 (cf. Fig. 6), in order to measure the current I_{cc2}. The equivalent inductance L_{eq}, equivalent of the inductances L_{g1} and L_{AC} in series, both in parallel with L_{g2}, is given by:
$$L_{eq} = \frac{V}{I_{cc2}\omega} \tag{5}$$
with:
$$L_{eq} = \frac{L_{g2}(L_{g1}+L_{AC})}{L_{g1}+L_{g2}+L_{AC}} \tag{6}$$
Therefore, the inductance L_{AC} is given by
$$L_{AC} = \frac{L_{g2}L_{eq}}{L_{g2}-L_{eq}} - L_{g1} \tag{7}$$
This inductance is also calculated with a short-circuit at bus 19, to check the equivalences of the two results.

3) State-space formulation: The dynamic equations of the control model are, in dq coordinates:

$$\begin{aligned}&\tfrac{di_{1d}}{dt}L_{S1}(Y_{1,1} - \tfrac{Y_{AC}^2}{Y_{2,1}}) = i_{1d}R_{S1}(\tfrac{Y_{AC}^2}{Y_{2,1}} - Y_{1,2})\\ &+i_{1q}\omega L_{S1}(Y_{1,1} - \tfrac{Y_{AC}^2}{Y_{2,1}}) + i_{2d}Y_{AC}R_{S2}(1 - \tfrac{Y_{2,2}}{Y_{2,1}})\\ &+v_{DC1}\tfrac{1}{2}\beta_{1d}(\tfrac{Y_{AC}^2}{Y_{2,1}} - Y_{1,2}) + v_{DC2}\tfrac{1}{2}\beta_{2d}Y_{AC}(1 - \tfrac{Y_{2,2}}{Y_{2,1}})\\ &+E(\tfrac{m_1}{L_{g1}} + \tfrac{m_2Y_{AC}}{L_{g2}Y_{2,1}})\end{aligned} \tag{8}$$

$$\begin{aligned}&\tfrac{di_{1q}}{dt}L_{S1}(Y_{1,1} - \tfrac{Y_{AC}^2}{Y_{2,1}}) = -i_{1d}\omega L_{S1}(Y_{1,1} - \tfrac{Y_{AC}^2}{Y_{2,1}})\\ &+i_{1q}R_{S1}(\tfrac{Y_{AC}^2}{Y_{2,1}} - Y_{1,2}) + i_{2q}Y_{AC}R_{S2}(1 - \tfrac{Y_{2,2}}{Y_{2,1}})\\ &+v_{DC1}\tfrac{1}{2}\beta_{1q}(\tfrac{Y_{AC}^2}{Y_{2,1}} - Y_{1,2}) + v_{DC2}\tfrac{1}{2}\beta_{2q}Y_{AC}(1 - \tfrac{Y_{2,2}}{Y_{2,1}})\end{aligned} \tag{9}$$

$$\begin{aligned}&\tfrac{di_{2d}}{dt}L_{S2}(Y_{2,1} - \tfrac{Y_{AC}^2}{Y_{1,1}}) = i_{1d}Y_{AC}R_{S1}(1 - \tfrac{Y_{1,2}}{Y_{1,1}})\\ &+i_{2d}R_{S2}(\tfrac{Y_{AC}^2}{Y_{1,1}} - Y_{2,2}) + i_{2q}\omega L_{S2}(Y_{2,1} - \tfrac{Y_{AC}^2}{Y_{1,1}})\\ &+v_{DC1}\tfrac{1}{2}\beta_{1d}Y_{AC}(1 - \tfrac{Y_{1,2}}{Y_{1,1}}) + v_{DC2}\tfrac{1}{2}\beta_{2d}(\tfrac{Y_{AC}^2}{Y_{1,1}} - Y_{2,2})\\ &+E(\tfrac{m_2}{L_{g2}} + \tfrac{m_1Y_{AC}}{L_{g1}Y_{1,1}})\end{aligned} \tag{10}$$

$$\begin{aligned}&\tfrac{di_{2q}}{dt}L_{S2}(Y_{2,1} - \tfrac{Y_{AC}^2}{Y_{1,1}}) = i_{1q}Y_{AC}R_{S1}(1 - \tfrac{Y_{1,2}}{Y_{1,1}})\\ &-i_{2d}\omega L_{S2}(Y_{2,1} - \tfrac{Y_{AC}^2}{Y_{1,1}}) + i_{2q}R_{S2}(\tfrac{Y_{AC}^2}{Y_{1,1}} - Y_{2,2})\\ &+v_{DC1}\tfrac{1}{2}\beta_{1q}Y_{AC}(1 - \tfrac{Y_{1,2}}{Y_{1,1}}) + v_{DC2}\tfrac{1}{2}\beta_{2q}(\tfrac{Y_{AC}^2}{Y_{1,1}} - Y_{2,1})\end{aligned} \tag{11}$$

$$\tfrac{dv_{DC1}}{dt} = \tfrac{3}{2C_1}(i_{1d}\beta_{1d} + i_{1q}\beta_{1q}) - \tfrac{2}{C_1}i_{DC} \tag{12}$$

$$\tfrac{dv_{DC2}}{dt} = \tfrac{3}{2C_2}(i_{2d}\beta_{2d} + i_{2q}\beta_{2q}) + \tfrac{2}{C_2}i_{DC} \tag{13}$$

$$\tfrac{di_{DC}}{dt} = \tfrac{1}{2L_{DC}}v_{DC1} - \tfrac{1}{2L_{DC}}v_{DC2} - \tfrac{r_{DC}}{L_{DC}}i_{DC} \tag{14}$$

where suffix numbers refer to the converter station, (i_{1d}, i_{1q}) and (i_{2d}, i_{2q}) are the grid currents. v_{DC1} and v_{DC2} are the DC voltages. i_{DC} is the DC line current. (β_{1d}, β_{1q}) and (β_{2d}, β_{2q}) are the control inputs of the VSCs. These variables are identical to the real model variables and can be measured locally. $Y_{1,1}$, $Y_{2,1}$, $Y_{1,2}$, $Y_{2,2}$ and Y_{AC} are defined by:

$$\begin{aligned}Y_{1,1} &= \tfrac{1}{L_{S1}} + \tfrac{m_1^2}{L_{g1}} + \tfrac{m_1^2}{L_{AC}} \quad Y_{2,1} = \tfrac{1}{L_{S2}} + \tfrac{m_2^2}{L_{g2}} + \tfrac{m_2^2}{L_{AC}}\\ Y_{1,2} &= m_1^2(\tfrac{1}{L_{g1}} + \tfrac{1}{L_{AC}}) \quad Y_{2,2} = m_2^2(\tfrac{1}{L_{g2}} + \tfrac{1}{L_{AC}})\\ Y_{AC} &= \tfrac{m_1m_2}{L_{AC}}\end{aligned} \tag{15}$$

The reactive powers of both side (Q_1 and Q_2) and the active power of of the right side (P_1) are given by:

$$\begin{aligned}Q_1 &= \tfrac{3}{4}v_{DC1}(\beta_{1q}i_{1d} - \beta_{1d}i_{1q})\\ P_2 &= \tfrac{3}{4}v_{DC2}(\beta_{2d}i_{2d} + \beta_{2q}i_{2q})\\ Q_2 &= \tfrac{3}{4}v_{DC2}(\beta_{2q}i_{2d} - \beta_{2d}i_{2q})\end{aligned} \tag{16}$$

A state-space model can be derived from (8)-(14) and (16):

$$\dot{x} = f(x,u) \qquad y = g(x,u) \tag{17}$$

where $x \in \Re^{n\times 1}$, $u \in \Re^{m\times 1}$ and $y \in \Re^{p\times 1}$. f and g are nonlinear functions and:

$x = \begin{bmatrix} i_{1d} & i_{1q} & i_{2d} & i_{2q} & v_{DC1} & v_{DC2} & i_{DC}\end{bmatrix}^T$

$u = \begin{bmatrix} \beta_{1d} & \beta_{1q} & \beta_{2d} & \beta_{2q}\end{bmatrix}^T$

$y = \begin{bmatrix} v_{DC1} & Q_1 & P_2 & Q_2\end{bmatrix}^T$

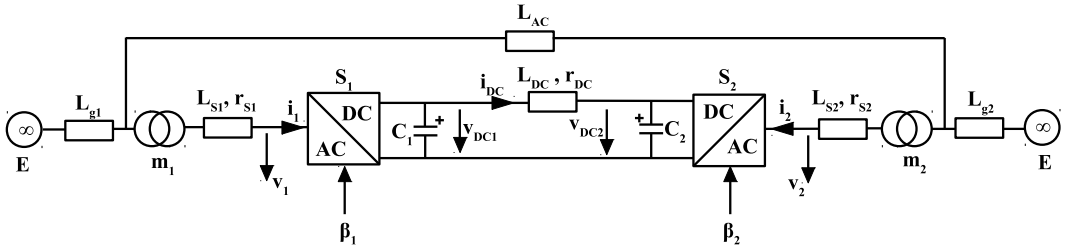

Fig. 3. Control Model Scheme

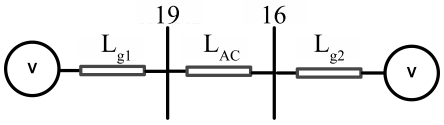

Fig. 4. Equivalent grid around buses 19 and 16

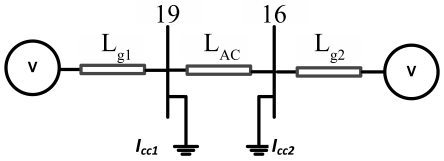

Fig. 5. Short-circuits applied at buses 19 and 16

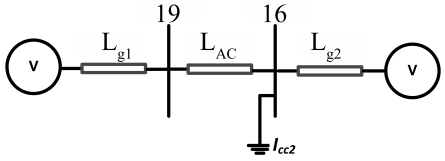

Fig. 6. Short-circuit applied at bus 16

B. Proposed MPC Controller Strategy

This subsection is focused on the controller strategy used to fit the objectives listed in section III. The full strategy is detailed in [3], where proof of stability, constraint enforcement and reference tracking is also given. The following brief record only aims at grasping the main ideas of this strategy.

The system is linearised in the neighbourhood of an operating point, augmented by integrators and sampled at a sample time of $10\mu s$ [3]. The system obtained is :

$$\dot{X_s} = A_s X_s + B_s U_s \qquad Y_s = C_s X_s \tag{18}$$

where X_s, U_s and Y_s are the linearized, augmented and sampled state, control signal and output respectively. Note that Y_s contains the linearized states of x. A_s, B_s and C_s are the new state-space matrices. U_{min} and U_{max} will denote respectively the minimum and maximum constraints on the control, taken from (2) and shifted by the operating point. Similarly, Y_{min} and Y_{max} will denote the constraints on the output described in (3). The MPC controller is defined by:

$$U_s(k) = F(k) X_s(k) \tag{19}$$

where k is the discrete step and F is the controller gain. F is computed at each discrete step by minimization of the following quadratic criterion:

$$\begin{aligned} J_\infty(k) = \textstyle\sum_{i=0}^{\infty} & X_s(k+i|k)^T Q X_s(k+i|k) \\ & + U_s(k+i|k)^T R U_s(k+i|k) \end{aligned} \tag{20}$$

where $Q > 0$ and $R > 0$ are weighting matrices for the tracking error and the control effort respectively. Thus, the closed-loop system at step k is:

$$\begin{aligned} X_s(k+1) &= (A_s + B_s F(k)) X_s(k) \\ Y_s(k) &= C_s X_s(k) \end{aligned} \tag{21}$$

The solving of the following LMIs optimization problem at each step ensures the stability, the minimization of J_∞, and the enforcement of the constraints on the input and state :

$$\min_{\gamma, Z, Y, W} \gamma \tag{22}$$

subject to,

$$Z \geq 0 \tag{23a}$$

$$\begin{bmatrix} 1 & \star \\ X_s(k) & Z \end{bmatrix} \geq 0 \tag{23b}$$

$$\begin{bmatrix} Z & \star & \star & \star \\ A_s Z + B_s Y & Z & \star & \star \\ Q^{\frac{1}{2}} Z & 0 & \gamma I_n & \star \\ R^{\frac{1}{2}} Y & 0 & 0 & \gamma I_m \end{bmatrix} \geq 0 \tag{23c}$$

$$\begin{bmatrix} W & \star \\ Y^T & Z \end{bmatrix} \geq 0, \quad W_{ii} \leq U_{sat,i}^2 \tag{23d}$$

$$\begin{bmatrix} Z & \star \\ C_{s,j}(A_s Z + B_s Y) & Y_{sat,j}^2 \end{bmatrix} \geq 0 \tag{23e}$$

where $\star$ symbol denotes symmetry of the matrix. $i = 1, \ldots, m$, $j = 1, \ldots, n$. γ, Z, Y, and W are decision variables obtained by solving the optimization problem, and:

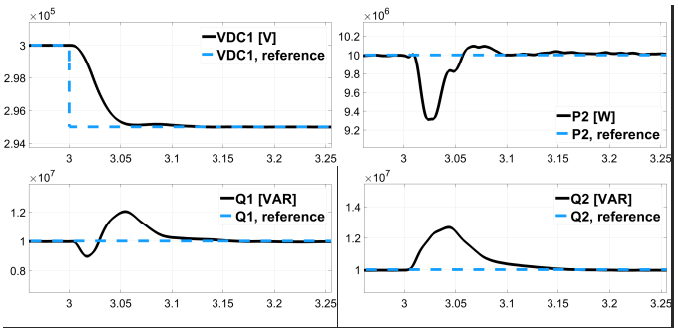

Fig. 7. Outputs and references, step on the reference of v_{DC1} (RMS).

$$C_s = \begin{bmatrix} C_{s,1} & \dots & C_{s,n} \end{bmatrix}^T$$
$$U_{sat} = \begin{bmatrix} U_{sat,1} & \dots & U_{sat,m} \end{bmatrix}^T$$
$$Y_{sat} = \begin{bmatrix} Y_{sat,1} & \dots & Y_{sat,n} \end{bmatrix}^T$$

U_{sat} and Y_{sat} are obtained using a support controller [23], that deals with asymmetrical constraints by selecting for each optimization the closest constraint to enforce. $F(k)$ is then calculated as follows:

$$F(k) = YZ^{-1} \tag{24}$$

V. Simulations and Results

In this section, the MPC strategy depicted in section IV is applied in EMT to the HVDC link embedded in the NE meshed grid, and compared to conventional control, i.e. vector control (see e.g. [24]).

Since the stability and reference tracking performances are studied here, four simulations with MPC controller are depicted, each performing a step on a different output (constraint enforcement is shown in [3]). Before each step, the system is at an equilibrium point with:

$$x = \begin{bmatrix} -67 & -68 & 67 & -68 & 300e3 & 301e3 & -31 \end{bmatrix}^T$$
$$u = \begin{bmatrix} 0.58 & 0.01 & 0.6 & -0.0045 \end{bmatrix}^T$$
$$y = \begin{bmatrix} 300e3 & 10e6 & 10e6 & 10e6 \end{bmatrix}^T$$

The steps are performed at time $3s$. The step on the output v_{DC1} is shown on Fig. 7 (output) and 8 (control signals). Outputs are shown for the steps on Q_1, P_2 and Q_2, respectively in Fig. 9, 10 and 11, in RMS values. The amplitude of the steps are respectively of 5kV, 5MVAR, 10MW, 5MVAR. The 95% response time of the controller for each step is about $100ms$, which fits the criterion 2 of section III.

The MPC is compared with the vector control subject to the same test case. As for the MPC, its time response is set to about $100ms$ For example, here is shown the output v_{DC1} for a step on the reference of v_{DC1} in Fig. 12. The output P_2 for a step on the reference of P_2 is shown in Fig. 13. The MPC leads to less overshoot than the vector control strategy, for the same response time tuning. Note that a reduction of a vector control overshoot would affect its response time.

Hence, the MPC shows a good dynamic behaviour and reference tracking, for a VDC-HVDC link embedded in a medium-scale meshed grid. These results shows the adequacy of the proposed control strategy in a realistic, EMT environment.

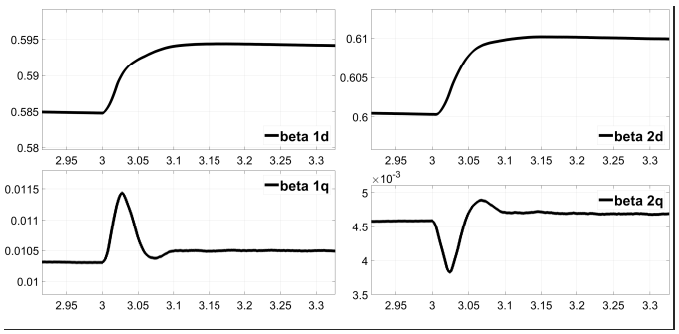

Fig. 8. Control signals, step on the reference of v_{DC1} (RMS).

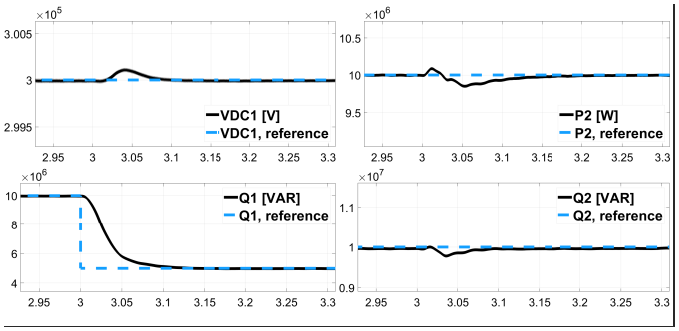

Fig. 9. Outputs and references, step on the reference of Q_1 (RMS).

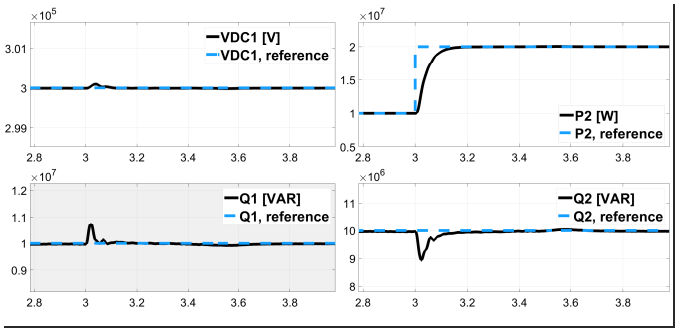

Fig. 10. Outputs and references, step on the reference of P_2 (RMS).

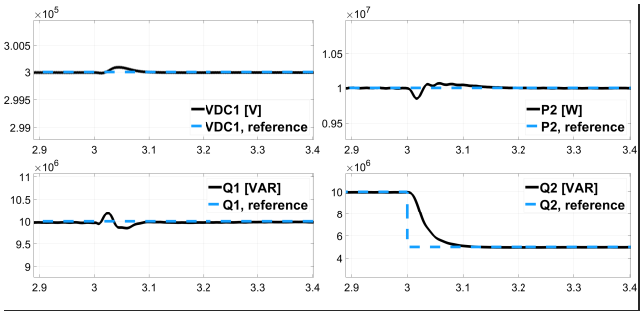

Fig. 11. Outputs and references, step on the reference of Q_2 (RMS).

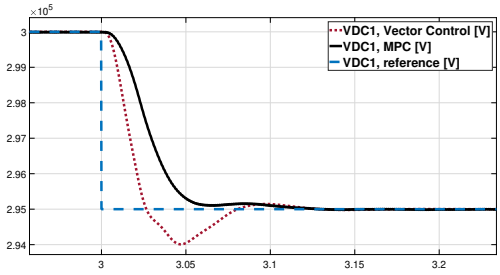

Fig. 12. v_{DC1} with vector control or MPC, and reference, step on the reference of v_{DC1} (RMS).

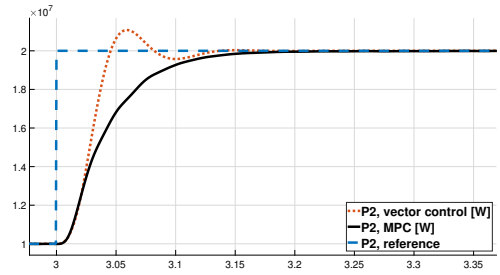

Fig. 13. P_2 with vector control or MPC, and reference, step on the reference of P_2 (RMS).

VI. Conclusion

In this paper, stabilization of HVDC system embedded into an AC grid with restricted states and controls is given by a MPC controller. The latter is synthesized taken into account not only the HVDC model but also characteristics of the neighbour grid. Compared to classic vector control, closed-loop stability is rigorously ensured by sufficient conditions in the format of LMIs and including actuator constraints in their general asymmetric form. Detailed EMT simulations proved the effectiveness and tracking performance of the proposed controller.

Further research will be focused on improving post-fault response, and robustness against parameters uncertainties. This can be done by fuzzification (e.g. [7]).

References

[1] F. Schettler, H. Huang, and N. Christl, "HVDC transmission systems using voltage sourced converters design and applications," in 2000 Power Eng. Soc. Summer Meeting, vol. 2, July 2000, pp. 715–720.

[2] L. Arioua and B. Marinescu, "Multivariable control with grid objectives of an HVDC link embedded in a large-scale ac grid," Int. J. of Elect. Power and Energy Syst., vol. 72, pp. 99–108, 2015.

[3] E. Thau, E. Kamal, B. Marinescu, and G. Denis, "Model predictive control of vsc-hvdc embedded into ac grid subject to state and control constraints," in 2019 IEEE Milan PowerTech, 2019, pp. 1–6.

[4] G. Asplund, "Application of HVDC light to power system enhancement," in 2000 IEEE Power Eng. Soc. Winter Meeting. Conf. Proc., vol. 4, Jan 2000, pp. 2498–2503.

[5] G. Zhang and Z. Xu, "Steady-state model for VSC based HVDC and its controller design," in 2001 IEEE Power Eng. Soc. Winter Meeting. Conf. Proc., vol. 3, Jan 2001, pp. 1085–1090.

[6] E. Kamal, A. Aitouche, and M. Oueidat, "Fuzzy fault-tolerant control of wind-diesel hybrid systems subject to sensor faults," IEEE Trans. on Sustainable Energy, vol. 4, no. 4, pp. 857–866, Oct 2013.

[7] E. Kamal, A. Aitouche, and D. Abbes, "Robust fuzzy scheduler fault tolerant control of wind energy systems subject to sensor and actuator faults," in Int. J. of Elect. Power and Energy Syst., vol. 55, 2014, pp. 402 – 419.

[8] S.-Y. Ruan, G.-J. Li, X.-H. Jiao, Y.-Z. Sun, and T. Lie, "Adaptive control design for VSC-HVDC systems based on backstepping method," Elect. Power Syst. Res., vol. 77, no. 5, pp. 559 – 565, 2007.

[9] Y. Matsuda and N. Ohse, "Simultaneous design of control systems with input saturation," Int. J. of Innovative Comput., Inform. and Control, vol. 4, no. 9, pp. 2205–2220, 2008.

[10] A. Saberi, A. A. Stoorvogel, and P. Sannuti, Control of Linear Systems with Regulation and Input Constraints. Commun. and Control Eng.. London, UK: Springer, 2003.

[11] S. Tarbouriech, I. Queinnec, and G. Garcia, "Stability region enlargement through anti-windup strategy for linear systems with dynamics restricted actuator," Int. J. of Syst. Sci., vol. 37, no. 2, pp. 79–90, 2006.

[12] G. A. Papafotiou, G. D. Demetriades, and V. G. Agelidis, "Technology readiness assessment of model predictive control in medium- and high-voltage power electronics," IEEE Trans. on Ind. Electron., vol. 63, no. 9, pp. 5807–5815, Sept 2016.

[13] S. Vazquez, J. Rodriguez, M. Rivera, L. G. Franquelo, and M. Norambuena, "Model predictive control for power converters and drives: Advances and trends," IEEE Trans. on Ind. Electron., vol. 64, no. 2, pp. 935–947, Feb 2017.

[14] Z. Yu, S. Huang, Z. Ma, and G. Chen, "Identification of critical lines in power grid based on electric betweenness entropy," in 2015 IEEE PES Asia-Pacific Power and Energy Eng. Conf., 2015, pp. 1–5.

[15] I. Munteanu, B. Marinescu, and F. Xavier, "Study of interactions between close hvdc links inserted in an ac grid: A mixed nonlinear and modal analysis approach," Int. Trans. on Elect. Energy Syst., vol. 30, no. 4, p. e12266, 2020.

[16] S. Bacha, I. Munteanu, and A. I. Bratcu, Power Electronic Converters Modeling and Control, ser. Adv. Textbooks in Control and Signal Process. London, U.K.:Springer, 2014, vol. 454.

[17] E. Kamal, M. Oueidat, A. Aitouche, and R. Ghorbani, "Robust scheduler fuzzy controller of DFIG wind energy systems," IEEE Trans. on Sustainable Energy, vol. 4, no. 3, pp. 706–715, July 2013.

[18] E. Kamal, A. Aitouche, R. Ghorbani, and M. Bayart, "Robust fuzzy fault-tolerant control of wind energy conversion systems subject to sensor faults," IEEE Trans. on Sustainable Energy, vol. 3, no. 2, pp. 231–241, April 2012.

[19] E. Kamal and A. Aitouche and R. Ghorbani and M. Bayart, "Intelligent control of wecs subject to parameter uncertainties, actuator and sensor faults," Acta Press, Control and Intelligent Syst., vol. 40, no. 3, pp. 1–9, 2012.

[20] E. Kamal and A. Aitouche and R. Ghorbani and M. Bayart, "Robust fuzzy logic control of wind energy conversion systems with unknown inputs," Acta Press, Int. J. Power and Energy Syst., vol. 32, no. 2, pp. 71–81, 2012.

[21] E. Kamal and A. Aitouche and R. Ghorbani and M. Bayart, "Robust nonlinear control of wind energy conversion systems," Int. J. of Elect. Power and Energy Syst., vol. 44, no. 1, pp. 202 – 209, 2013.

[22] L. Arioua, B. Marinescu, and E. Monmasson, "Control of high voltage direct current links with overall large-scale grid objectives," IET Gener., Transmiss. Distribution, vol. 8, no. 5, pp. 945–956, 2014.

[23] J. Oravec, M. Kvasnica, and M. Bakosova, "Quasi-non-symmetric input and output constraints in lmi-based robust mpc," IFAC-PapersOnLine, vol. 50, no. 1, pp. 11 337 – 11 342, 2017, 20th IFAC World Congr.

[24] V. Sood and H. Patel, "Comparison between direct and vector control strategy for vsc-hvdc system in emtp-rv," in 2010 Joint Int. Conf. on Power Electron., Drives and Energy Syst. 2010 Power India, 2010, pp. 1–6.